

# Slope of the upper critical field at $T_c$ in two-band superconductors with nonmagnetic disorder: $s_{++}$ superconductivity in $\text{Ba}_{1-x}\text{K}_x\text{Fe}_2\text{As}_2$

R. Prozorov<sup>1,2,\*</sup>, V. G. Kogan<sup>1</sup>, M. Kończykowski<sup>3</sup>, and M. A. Tanatar<sup>1,2</sup>

<sup>1</sup>Ames National Laboratory, Ames, Iowa 50011, USA

<sup>2</sup>Department of Physics & Astronomy, Iowa State University, Ames, Iowa 50011, USA

<sup>3</sup>Laboratoire des Solides Irradiés, CEA/DRF/IRAMIS, École Polytechnique, CNRS, Institut Polytechnique de Paris, F-91128 Palaiseau, France



(Received 22 June 2023; revised 2 September 2023; accepted 15 December 2023; published 10 January 2024)

A recent theory of the disorder-dependent slope of the upper critical field at the superconducting transition temperature  $T_c$ , defined as  $S \equiv |dH_{c2}/dT|_{T \rightarrow T_c}$ , is extended to multiband superconductors aimed at iron-based superconductors, considering two constant gaps of different magnitudes and, potentially, different signs. We show that the slope  $S$  decreases with increasing nonmagnetic scattering rate  $P$  in the  $s_{\pm}$  pairing state and increases in the  $s_{++}$  superconductor for a reasonable range of parameters. The experiment shows that in a typical iron-based superconductor,  $\text{Ba}_{1-x}\text{K}_x\text{Fe}_2\text{As}_2$  (BaK122), the nonmagnetic disorder induced by electron irradiation leads to an increasing  $S(P)$  across the superconducting “dome,” at different  $x$ . This implies that  $\text{Ba}_{1-x}\text{K}_x\text{Fe}_2\text{As}_2$  is likely an  $s_{++}$  superconductor with two effective gaps of different magnitudes, at least at moderate doping levels,  $x < 0.6$ . This work reopens a decade-long discussion about the nature of the superconducting order parameter in iron pnictides.

DOI: [10.1103/PhysRevB.109.024506](https://doi.org/10.1103/PhysRevB.109.024506)

## I. INTRODUCTION

Soon after discovering iron-based superconductors (IBSs), it became clear that although practically all these materials are fully gapped, measured thermodynamic quantities did not follow the clean single isotropic gap predictions. Instead, it was found that the natural and deliberately introduced nonmagnetic disorder is pair breaking [1,2]. Throughout this paper we use the dimensionless scattering rate  $P = \hbar/(2\pi T_{c0}\tau)$ , where  $T_{c0}$  is the transition temperature in the clean limit and  $\tau$  is the transport scattering time. Even in the clean limit (achievable in iron pnictides due to the extremely short coherence length of 2–3 nm [3]), the addition of nonmagnetic disorder led to significant suppression of the transition temperature  $T_c$ , violating the Anderson theorem [4]. Based on earlier work [5], Mazin *et al.* suggested the so-called  $s_{\pm}$  pairing due to spin fluctuations promoted by nesting [6]. At the same time, Kuroki *et al.* have also proposed an  $s_{\pm}$  pairing scenario [7]. Angle-resolved photoemission spectroscopy (ARPES) revealed a complex anisotropic doping-dependent electronic band structure with multiple energy gaps of different magnitude [8–13]. Subsequently, the original nesting-driven picture was generalized to include states where nesting does not play a pivotal role, but still the order parameter changes its sign between some of the Fermi surface sheets; see, for reviews, Refs. [14–19].

At the same time, the  $s_{++}$  pairing was not dismissed [11,20,21]. It was shown that the results of transport and thermodynamic measurements could be explained using both anisotropic  $s_{\pm}$ , and  $s_{++}$  pairing due to spin and orbital fluctuations, respectively [20]. Moreover, a crossover from  $s_{\pm}$  to  $s_{++}$

was predicted [22] and observed [23]. Furthermore, the effect of nonmagnetic impurities on the neutron scattering spectrum was successfully analyzed within an  $s_{++}$  scenario [24].

In most IBSs, including the subject of this study,  $\text{Ba}_{1-x}\text{K}_x\text{Fe}_2\text{As}_2$  (BaK122),  $T_c(x)$  values show a domelike variation. However, the slope of the upper critical field,  $S \equiv |dH_{c2}/dT|_{T \rightarrow T_c}$ , in pristine samples, appears to be a linear function of  $T_c$ , as expected from the Bardeen-Cooper-Schrieffer (BCS) theory in the clean limit [25]. The slope  $S$  is considered a very useful quantity because it is used to estimate the zero-temperature value of the upper critical field,  $H_{c2}(0)$ , which is experimentally mostly inaccessible in IBSs. For example, one can estimate the coherence length from  $H_{c2}(0)$  and discuss possible Pauli limiting. However, the Helfand-Werthamer (HW) [26,27] or more often quoted Werthamer-Helfand-Hohenberg (WHH) [28] theory was developed for isotropic  $s$ -wave superconductors. Their theory does not apply to anisotropic superconductivity, which was considered by Pokrovsky and Pokrovsky [29] and recently cast in a more accessible form in Ref. [25]. Here we extend the latter approach even further to the two-band superconductivity and apply it to analyze the data obtained in electron-irradiated hole-doped BaK122 crystals.

There are numerous reports on the slope of the upper critical field at  $T_c$  as a function of disorder introduced by various means in various materials. The overall experimental picture is quite clear: Superconductors with line nodes show that disorder  $P$  suppresses the slope, whereas those without nodes show an increasing  $S(P)$ . The first and most studied two-gap  $s_{++}$  superconductor,  $\text{MgB}_2$ , shows an increase of  $S$  with increasing residual resistivity [30]. In another proven two-gap superconductor,  $\text{V}_3\text{Si}$  [31], a pronounced increase of  $S(P)$  was found after neutron irradiation [32]. On the line nodal

\*Corresponding author: [prozorov@ameslab.gov](mailto:prozorov@ameslab.gov)

side, we have high- $T_c$  cuprates: hole-doped  $\text{YBa}_2\text{Cu}_3\text{O}_{7-x}$  (YBCO) [33] and electron-doped  $(\text{NdCe})_2\text{CuO}_{4+y}$  [34]. For quite some time, electron-doped cuprates were contrasted with hole-doped ones as being fully gapped. In YBCO, a  $T$ -linear variation of the London penetration depth,  $\lambda(T)$ , meant the existence of line nodes [35], but in electron-doped superconductors, it took seven more years before a similar but weaker claim was made, based on the quadratic behavior of  $\lambda(T)$ , characteristic of dirty nodal superconductors [36]. Now we can say that this is confirmed by the measured decrease of  $S(P)$  [34].

In IBSs, the transition temperature decreases with nonmagnetic disorder. An example is a study of the electron-doped  $\text{Ba}(\text{Fe}_{1-x}\text{Co}_x)_2\text{As}_2$ , where disorder was introduced by ball-milling [37]. A similar effect is found in hole-doped  $\text{Ba}_{1-x}\text{K}_x\text{Fe}_2\text{As}_2$  IBSs after fast neutron irradiation [38] and 2.5 MeV electron irradiation (this work); see also Ref. [39]. This suppression of  $T_c$  by disorder is well described by the extension of the Abrikosov-Gor'kov (AG) theory of magnetic impurities in conventional single-band isotropic  $s$ -wave superconductors [40] to the anisotropic order parameter, including  $s_{++}$  and  $s_{\pm}$  pairing [41–43].

With regard to the slope  $S$ , a steady decrease was found in isovalently substituted  $\text{BaFe}_2(\text{As}_{1-x}\text{P}_x)_2$ . In a heavily electron-irradiated sample,  $T_c$  was suppressed below 10 K, while the slope  $S$  monotonically decreased with the irradiation dose [44]. However, this particular IBS is unique among 122 compounds: it is nodal [45], and the observed decrease is consistent with our results. Another IBS,  $\text{NdFeAs}(\text{O},\text{F})$ , showed a monotonic increase in  $|dH_{c2}/dT|$  upon irradiation with alpha particles [46]. In the IBS of interest here,  $\text{Ba}_{1-x}\text{K}_x\text{Fe}_2\text{As}_2$ , strain and doping were shown to increase  $S$  [47]. Fast neutron irradiation led to a substantial increase in  $S$  in the optimally

doped and underdoped compositions and an unclear change on the overdoped side [38]. Importantly, these experiments showed that the  $ab$ -plane and the  $c$ -axis  $H_{c2}$  were affected similarly by disorder.

In this paper, we extend the single-band theory of Ref. [25] to a two-band scenario needed to describe the iron-based superconductors. Numerical solutions show that, practically in the entire domain of a sign-changing order parameter, the slope  $S$  decreases with  $P$ . Analyzing the data collected on electron-irradiated BaK122, we conclude that, barring some unrealistic set of parameters, having a slope  $S$  that *increases* with  $P$  places the BaK122 in the  $s_{++}$  domain. This is an unorthodox conclusion, and we hope that our work will stimulate further studies.

## II. THE SLOPE OF $H_{c2}$ AT $T_c$

Let us assume the often used separation of variables in the order parameter [48],  $\Delta(\mathbf{k}, T) = \Psi(T)\Omega(\mathbf{k})$ , where the angular part is normalized via its Fermi surface average  $\langle \Omega^2 \rangle_{\text{FS}} = 1$  [49,50] and the  $\Psi(T)$  function is obtained from the self-consistency equation [51]. We call this an  $\Omega$  model. Without magnetic scattering, the critical temperature of materials is given by [41,42]

$$\ln t_c + (1 - \langle \Omega^2 \rangle) \left[ \psi \left( \frac{P/t_c + 1}{2} \right) - \psi \left( \frac{1}{2} \right) \right] = 0, \quad (1)$$

where  $t_c = T_c/T_{c0}$  and  $P$  is the dimensionless transport (nonmagnetic) scattering parameter (rate). Obviously, the Anderson theorem is readily recovered for isotropic  $s$ -wave superconductors, where  $\Omega = 1$ .

The slope of the upper critical field along the  $c$  axis of a uniaxial superconductor is given by [25,29]

$$\left. \frac{\partial H_{c2}}{\partial T} \right|_{T_c} = - \frac{8\pi\phi_0 T_{c0}}{\hbar^2} \frac{t_c \left[ 1 + (1 - \langle \Omega^2 \rangle) \psi' \left( \frac{1}{2} + \frac{P}{2t_c} \right) \right]}{h_{3,0} \langle \Omega^2 v_a^2 \rangle + 2(P/2t_c) h_{3,1} \langle \Omega \rangle \langle \Omega v_a^2 \rangle + (P/2t_c)^2 h_{3,2} \langle \Omega^2 \rangle \langle v_a^2 \rangle}, \quad (2)$$

where  $\psi$  is the digamma function,  $v_a$  is the in-plane Fermi velocity, and all coefficients  $h_{\mu,v}(x)$  are evaluated at  $x = P/2t_c$ . These coefficients are

$$\begin{aligned} h_{3,0} &= -\frac{1}{2} \psi'' \left( \frac{1}{2} + x \right), & h_{3,1} &= \frac{1}{x^3} \left[ \psi \left( \frac{1}{2} + x \right) - \psi \left( \frac{1}{2} \right) - x \psi' \left( \frac{1}{2} + x \right) + \frac{x^2}{2} \psi'' \left( \frac{1}{2} + x \right) \right], \\ h_{3,2} &= \frac{1}{2x^4} \left\{ \pi^2 x - 6 \left[ \psi \left( \frac{1}{2} + x \right) - \psi \left( \frac{1}{2} \right) \right] + 4x \psi' \left( \frac{1}{2} + x \right) - x^2 \psi'' \left( \frac{1}{2} + x \right) \right\}. \end{aligned} \quad (3)$$

## III. THE TWO-BAND MODEL

Iron pnictides generically have five bands that cross the Fermi level, but according to most studies, they host two effective distinct order parameters of possibly different signs [8–13]. Therefore a minimalistic two-gap model seems adequate for estimates. A macroscopic property, such as  $H_{c2}$  and its slope at  $T_c$ , is not sensitive to the details of the electronic band structure because, as seen from Eq. (2) for the slope  $S$ , these details enter via the averages over the whole Fermi surface. The order parameter  $\Delta(t, \mathbf{k}) = \Psi(T)\Omega(\mathbf{k})$ , and, in fact, only the angular part,  $\langle \Omega(\mathbf{k}) \rangle$  and its convolutions with the Fermi velocity (e.g.,  $\langle \Omega^2 v_F^2 \rangle$ ), is relevant for the slope  $S$ .

The full-blown two-band theory with three coupling constants and three potentially different scattering rates contains too many parameters, the effects of which on the slope of  $H_{c2}$  are not easy to determine. Hence we employ the simplest “minimum two-band model” within which we can calculate the slopes. This two-band  $\Omega$  model was first introduced for  $\text{MgB}_2$  to explain the temperature-dependent anisotropy of the London penetration depth [50]. Here, we adopt the same approach to analyze the slope of  $H_{c2}$  at  $T_c$ .

Let us consider two order parameters,  $\Omega_1$  and  $\Omega_2$ , residing in two bands with partial densities of states (DOSs) at the Fermi level,  $n_{1,2} = N_{1,2}/N$ , where  $N = N_1 + N_2$  is the total

density of states so that  $n_1 + n_2 = 1$ . The normalization equation reads [50]

$$\langle \Omega^2 \rangle = n_1 \langle \Omega_1^2 \rangle + n_2 \langle \Omega_2^2 \rangle = 1. \quad (4)$$

Simplifying Eq. (4) even further, considering  $\Omega_i$  to be constants (that can have different signs, though!) and introducing the ratio  $r = \Omega_2/\Omega_1$  and the ratio of the partial densities of states  $n = n_2/n_1$ , we obtain

$$\Omega_1^2 = \frac{1}{n_1 + n_2 r^2}, \quad \Omega_2^2 = \frac{r^2}{n_1 + n_2 r^2}. \quad (5)$$

Therefore the average, needed for Eq. (1), is

$$\langle \Omega \rangle^2 = \frac{(nr + 1)^2}{(n + 1)(nr^2 + 1)}, \quad (6)$$

and Eq. (1) for the transition temperature now reads

$$\ln t_c + \frac{n(r-1)^2}{(n+1)(nr^2+1)} \left[ \psi\left(\frac{P}{2t_c} + \frac{1}{2}\right) - \psi\left(\frac{1}{2}\right) \right] = 0. \quad (7)$$

We proceed in a similar way, expressing various averages in Eq. (2) for the slope of  $H_{c2}$  at  $T_c$ . Introducing the ratio  $v = v_{a2}/v_{a1}$  and assuming a simple cylindrical Fermi surface where  $v_{a1} = v_{F1} \cos \varphi$ ,  $v_{F1}$  being the Fermi velocity on band 1, we have

$$\langle \Omega \rangle = \frac{1 + nr}{\sqrt{(1+n)(1+nr^2)}}, \quad (8)$$

$$\langle \Omega^2 v_a^2 \rangle = \frac{v_{F1}^2}{2} \frac{1 + nr^2 v^2}{1 + nr^2}, \quad (9)$$

$$\langle \Omega v_a^2 \rangle = \frac{v_{F1}^2}{2} \frac{1 + nr v^2}{\sqrt{(1+n)(1+nr^2)}}, \quad (10)$$

$$\langle v_a^2 \rangle = \frac{v_{F1}^2}{2} \frac{1 + nv^2}{1 + n}, \quad (11)$$

where  $1/2$  comes from  $\langle \cos^2 \varphi \rangle = 1/2$  since we consider constant  $\Omega_i$  and only  $\cos^2 \varphi$  needs to be averaged. These equations are substituted into the general equation (2) along with the coefficients, Eq. (3), and the slope can be numerically evaluated for any values of  $n$ ,  $r$ , and  $v$ , characterizing the two-band superconductor, and for any nonmagnetic scattering rate  $P$ . When doing numerical calculations, one has to bear in mind that for some cases,  $T_c$  might turn zero at a finite  $P$ . For example, in a pure  $s_{\pm}$  situation, with  $n = 1$ ,  $v = 1$ , and  $r = -1$ ,  $T_c$  is suppressed to zero at  $P = 0.2808$ , the same value as for the  $d$ -wave order parameter, because in both cases  $\langle \Omega \rangle = 0$ .

Let us now examine some numerical solutions to the above equations. Figure 1 shows the transition temperature  $t_c$  at the critical value  $P = 0.2808$ , Eq. (1), varying the gap ratio  $r$  and the ratio of the partial densities of states,  $n$ . The ratio of Fermi velocities was found not to affect the results qualitatively; so we set  $v = 1$ . A clearly asymmetric three-dimensional (3D) surface, Fig. 1(a), shows a deep trench at negative  $r$  (gaps of opposite signs), corresponding to a suppression of  $t_c$  to zero. This can be better seen on the color density plot in Fig. 1(b). The two black lines correspond to  $t_c = 0.05$  ( $t_c$  cannot be set to zero due to the singularity in the derivative). The true  $t_c = 0$  line is located in between. By definition,  $t_c$  is suppressed to zero when  $\langle \Omega \rangle = 0$ , and from Eq. (8) we see that this line in the  $(n, r)$  plane satisfies the equation  $nr + 1 = 0$ , which

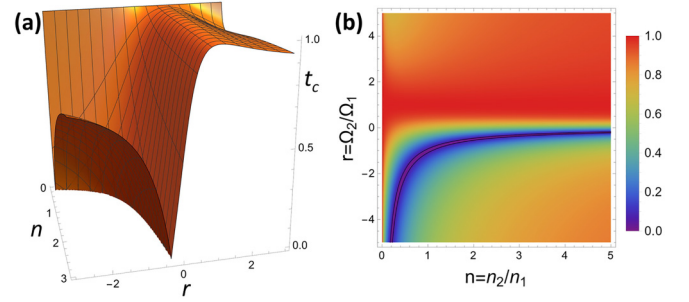


FIG. 1. Transition temperature normalized by its pristine value,  $t_c = T_c/T_{c0}$ , plotted as a function of  $n = n_2/n_1$  and  $r = \Omega_2/\Omega_1$ , in a 3D plot (a) and in a 2D color plot (b). The deep trench on the 3D plot (a), corresponding to the middle of the blue  $nr + 1 = 0$  curve in (b), is the line where  $t_c \rightarrow 0$ , according to Eqs. (1) and (8).

is what we have in Fig. 1. Except for this line, all positive values of  $n$  and both positive and negative values of  $r$  are possible. Of course, in realistic iron-based superconductors, the ratio of the two effective gaps (supported by five Fermi surface sheets) is about 2 [52] (or, equivalently for our model,  $1/2$ ). For positive  $r$ , expectedly,  $t_c$  does not change much but decreases for larger  $r$  since the anisotropy increases. From Fig. 1 it is obvious that for  $0 < n < 1$ , the maximum possible  $P$  is not much higher than the critical value. However, instead of a sharp termination, there is a long tail, with  $t_c$  practically at zero. For a larger  $n$ , a larger range of the scattering parameter can be explored.

Figure 2 shows 3D and 2D color plots of the slope  $S(P = 0.001, n, r, v = 1)$  in the clean limit. A fairly complicated surface reveals significant asymmetry with respect to the positive and negative values of  $r$ . Two contour lines in Fig. 2(b) show the location of  $S = 1$ . According to the color legend, the red domain between is where  $S > 1$ , and the value of  $S$  is lower around this domain. However, the magnitude of slope  $S$  does not tell us whether it increases or decreases with scattering  $P$ . To probe the disorder dependence of  $S$ , we construct the numerical derivative. In the clean limit we use  $dS/dP \approx [S(P = 0.011) - S(P = 0.010)]/0.001$  and plot this quantity in Fig. 3. Here, positive values indicate an increase in  $S$  with

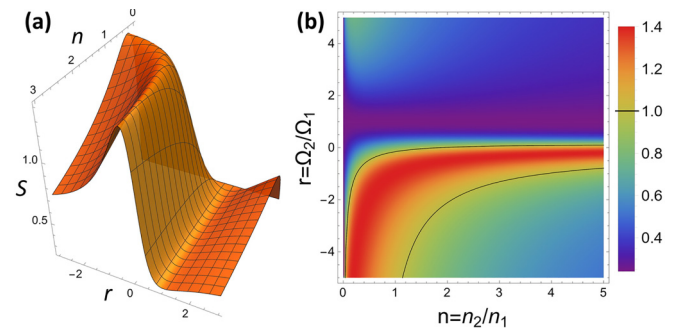


FIG. 2. The slope  $S$  plotted as a function of the ratio of the partial densities of states  $n = n_2/n_1$  and of the ratio of the angular parts of the order parameter  $r = \Omega_2/\Omega_1$  in a 3D plot (a) and in a 2D color plot (b). The region  $r > 0$  corresponds to  $s_{++}$  pairing, whereas the region  $r < 0$  corresponds to the  $s_{\pm}$  pairing. Clearly, the slope  $S$  behaves very differently in these two domains.

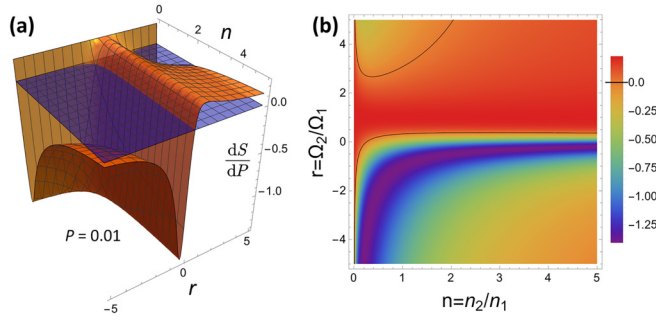


FIG. 3. Numerical derivative of the slope, using  $dS/dP \approx [S(P = 0.011) - S(P = 0.010)]/0.001$ , as a function of  $n$  and  $r$  in a 3D plot (a) and in a 2D color plot (b). Negative values indicate slopes decreasing with  $P$ , and positive values indicate slopes increasing with  $P$ . The two contour lines on the density plot (b) show  $S = 0$ .

an increase in  $P$ . Surprisingly, the result is nontrivial, showing different trends depending on  $n$  and  $r$ . A 2D density plot in Fig. 3(b) shows two black contour lines of  $S = 0$ , indicating a large positive domain (in red) for positive values of  $r$ . Above roughly  $r = 3$ , and  $n \sim 1$ , the high anisotropy takes over even in this  $s_{++}$  state, and  $S$  becomes a decreasing function of  $P$ . We note that we have also explored the influence of the ratio of Fermi velocities  $v$  but did not find much effect on the results.

However, considering our experimental results, it is more interesting to explore a possible slope increase on the negative,  $s_{\pm}$ , side of  $r$  values. Then, the only region of interest is at small  $n$ . Figure 4 zooms into this region and, in addition to the clean limit  $dS/dP$ , shows a dirty-limit derivative,  $dS/dP$ , offset by  $P = 0.1$  compared with the clean limit, about a third of the critical value of 0.2808. According to the color legend, the red domain is where the slope of  $S$  increases with increasing nonmagnetic scattering. This is only possible for  $n < 0.2$ . In iron pnictides, and more specifically,  $\text{Ba}_{1-x}\text{K}_x\text{Fe}_2\text{As}_2$ ,  $n \sim 1$ . Furthermore, with a fairly two-dimensional character of the bands, the densities of states are nearly independent of energy; therefore doping, while shifting the Fermi level, does not alter much the  $n$  values [54]. Regarding the gap ratio, it was found experimentally that  $|r| \approx 2$  (or, which is the same in our model,  $|r| \approx 1/2$ ) [8,12]. Therefore our model predicts that if iron pnictides were  $s_{\pm}$  superconductors, the slope at  $T_c$  of their upper critical field should decrease with increasing transport (nonmagnetic) scattering.

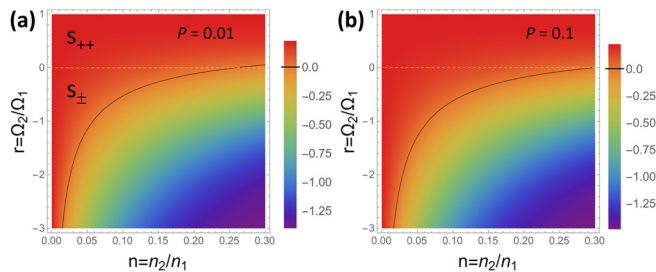


FIG. 4. Two numerical derivatives of the slope. (a) Same as in Fig. 3 (clean limit), but focusing on the region of small  $n$ . (b)  $dS/dP$  corresponding to a significant scattering rate,  $P = 0.1$ . In the narrow region indicated by the red color, a slope that is increasing with  $P$  exists in the  $s_{\pm}$  pairing region.

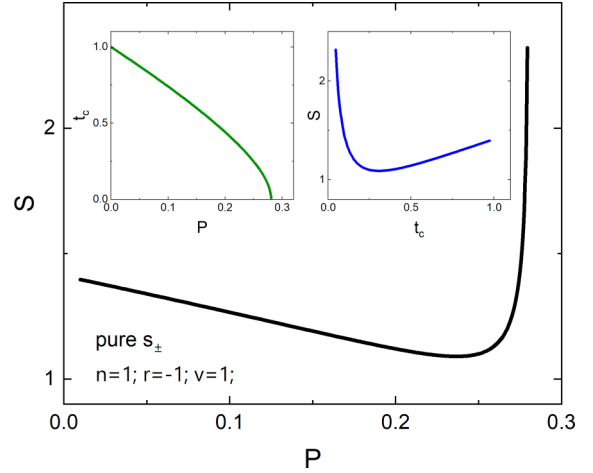


FIG. 5. The slope of the upper critical field for Mazin's [53]  $s_{\pm}$  state,  $n = 1$ ,  $v = 1$ , and  $r = -1$ . This is identical to a superconductor with a  $d$ -wave order parameter; see Fig. 3 in Ref. [25].

The expectations for a pure  $s_{\pm}$  state are, in fact, similar to a line nodal  $d$ -wave superconductor [25]. Figure 5 shows  $S(P)$  for the pure  $s_{\pm}$  state where  $n = 1$ ,  $v = 1$ , and  $r = -1$ . Similarly to a  $d$ -wave superconductor,  $T_c$  is suppressed to zero at the critical value  $P = 0.2808$  (upper left inset), at which the slope sharply diverges. As discussed in Ref. [25], there is a small interval where this state is gapless. The plot of  $S(P)$  is convenient for theory; however, in practice, one would use the observed transition temperature as a measure of the scattering rate. This is shown in the upper right inset. The slope is predicted to decrease for most  $T_c$  values.

Let us examine the region of the  $s_{\pm}$  side where the slope can increase, as discussed above, for  $n < 0.2$ . Figure 6 shows the curves taken at the fixed (experimental) value of  $r = -0.5$  for  $n = 0.01, 0.1$ , and  $0.2$ . Already at  $n = 0.2$ , the slope starts

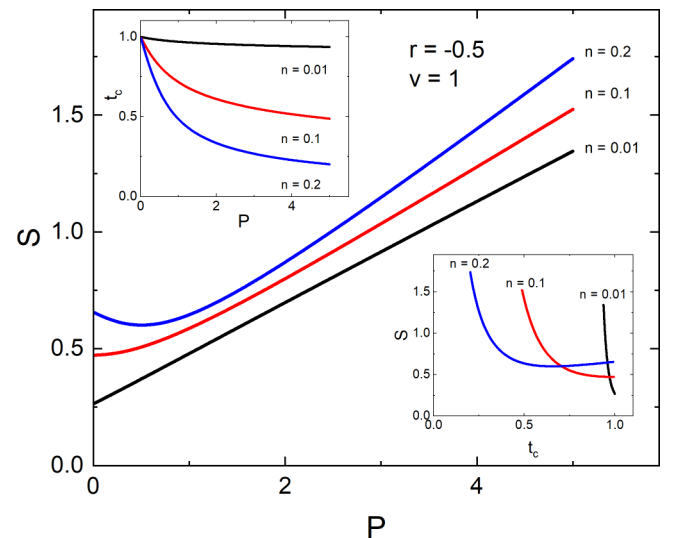


FIG. 6. The slope  $S$  for  $s_{\pm}$  pairing,  $r = -0.5$ ; in the narrow domain of small  $n = 0.01$  it increases with  $P$ , but it changes to a decreasing function already for  $n = 0.2$ . The insets show a corresponding reduction of the transition temperature for the same  $n$  values.

from the decreasing trend. The suppression of  $t_c$  is shown in the upper left inset, whereas the slope vs  $t_c$  is shown in the lower right inset. It is unlikely that this situation will occur in BaK122 at all levels of doping.

#### IV. EXPERIMENT

Single crystals of  $\text{Ba}_{0.2}\text{K}_{0.8}\text{Fe}_2\text{As}_2$  were grown by using an inverted temperature gradient method with starting materials of Ba and K lumps and Fe and As powders. Details of the growth are published elsewhere [55–57]. Resistivity measurements were performed in a standard four-probe configuration. Typical dimensions of the samples are  $(1\text{--}2) \times 0.5 \times (0.02\text{--}0.1)$   $\text{mm}^3$ . Silver wires of 50  $\mu\text{m}$  diameter were soldered to the sample to provide electrical contacts [58]. The sample with four contact wires attached was mounted on a hollowed Kyocera chip (for the electron beam to propagate) over a hole of about 5 mm diameter in the center. After receiving a certain dose, the Kyocera chip was extracted and mounted in a different cryostat without disturbing the sample or the contacts. After resistance vs temperature at different applied magnetic fields was measured, the Kyocera chip was returned to the irradiation chamber, and the process was repeated. The same procedure was performed on samples of different compositions.

The 2.5 MeV electron irradiation was performed at the SIRIUS Pelletron-type linear accelerator operating in the Laboratoire des Solides Irradiés at the École Polytechnique in Palaiseau, France. The acquired irradiation dose is conveniently measured in  $\text{C}/\text{cm}^2$ , where  $1 \text{ C}/\text{cm}^2 = 6.24 \times 10^{18}$  electrons/ $\text{cm}^2$ . A Faraday cup placed behind the sample chamber allowed an accurate measurement of the acquired dose during irradiation. Electron irradiation was performed in liquid hydrogen at 20 K to prevent Frenkel pair recombination and defect clustering. The typical concentration of the induced defects is one defect per 1000 unit cells. Here, our highest dose of  $8.93 \text{ C}/\text{cm}^2$  corresponds to approximately one defect per 22 conventional unit cells ( $Z = 2$  for  $\text{BaFe}_2\text{As}_2$ ). Details of the irradiation experiments are available elsewhere [39,59,60].

#### V. EXPERIMENTAL SLOPE, $|\partial H_{c2}/\partial T|_{T=T_c}$ , IN $\text{Ba}_{1-x}\text{K}_x\text{Fe}_2\text{As}_2$

As a specific system to probe our theoretical conclusions, we selected a well-studied  $(\text{Ba}_{1-x}\text{K}_x)\text{Fe}_2\text{As}_2$  family of iron-based superconductors (abbreviated as BaK122). Taking into account the significant dependence of the results on  $n$ , we have probed several compositions. An example of the data collected for overdoped BaK122,  $x = 0.56$ , is shown in Fig. 7, where temperature-dependent resistance is plotted for several values of the applied magnetic field. The inset shows a full temperature dependence of the resistance normalized by the room temperature value. The curves are parallel and not smeared, allowing us to use an easy criterion of 50% of the transition to estimate  $H_{c2}$ . We are interested in the functional dependence of the slope on the scattering parameter; so the precise values of  $H_{c2}$  are not important.

Four different compositions were measured,  $x = 0.2$  (underdoped),  $x = 0.34$  (optimally doped), and two moderately overdoped,  $x = 0.47$  and  $x = 0.56$ , but before the Lifshitz

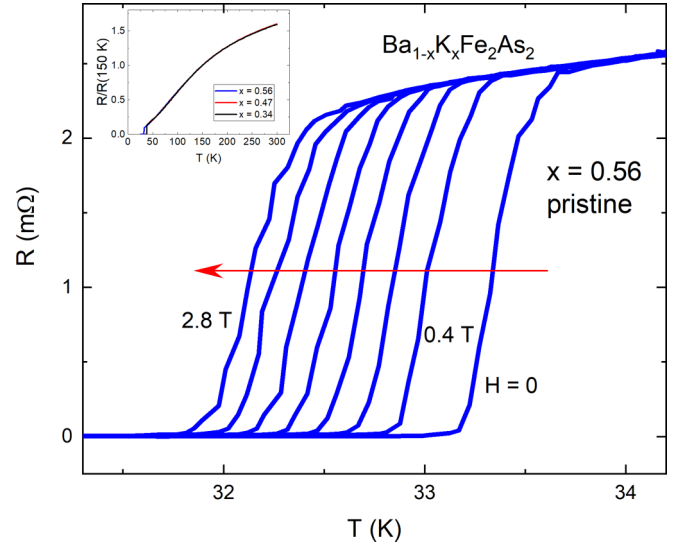


FIG. 7. Temperature-dependent resistance of a pristine sample of BaK122;  $x = 0.56$ . Data are taken in magnetic fields applied along the tetragonal  $c$  axis from 0 T (right curve) to 2.8 T (left curve). Note the nearly parallel shift of the curves, which makes the same slope of the  $H_{c2}(T)$  curve irrespective of the criterion used. The inset shows the temperature dependence of normalized resistance  $R/R(300 \text{ K})$  for compositions  $x = 0.34$  (black),  $x = 0.47$  (red), and  $x = 0.56$  (blue).

transition, which alters the electronic band structure and the gap structure considerably [57]. Each sample was measured as shown in Fig. 7, then irradiated with the dose shown, brought to room temperature, and again measured, and the cycle was repeated. The top panel of Fig. 8 shows the change

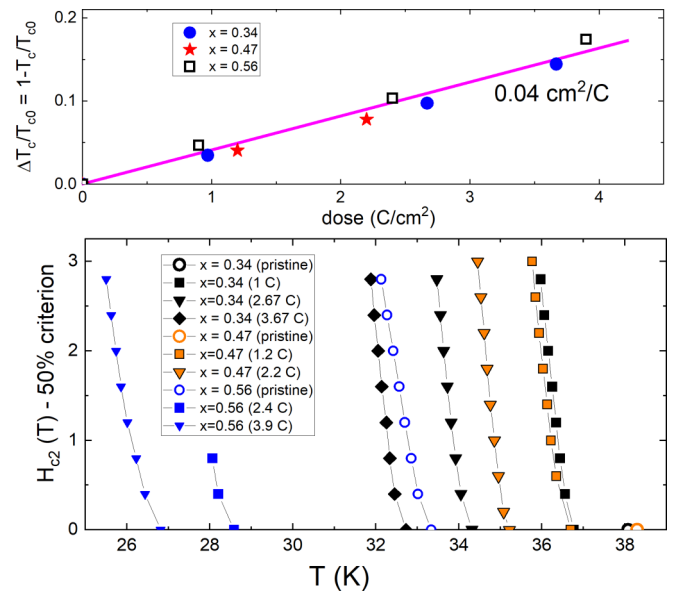


FIG. 8. Top: normalized variation of the transition temperature,  $\Delta T_c/T_{c0}$ , plotted vs the irradiation dose showing a universal behavior for all studied compositions because it depends only on the scattering rate  $P$ , which is a linear function of the dose. Bottom: the upper critical field as a function of temperature near  $T_c$  for select compositions, shown in the legend.

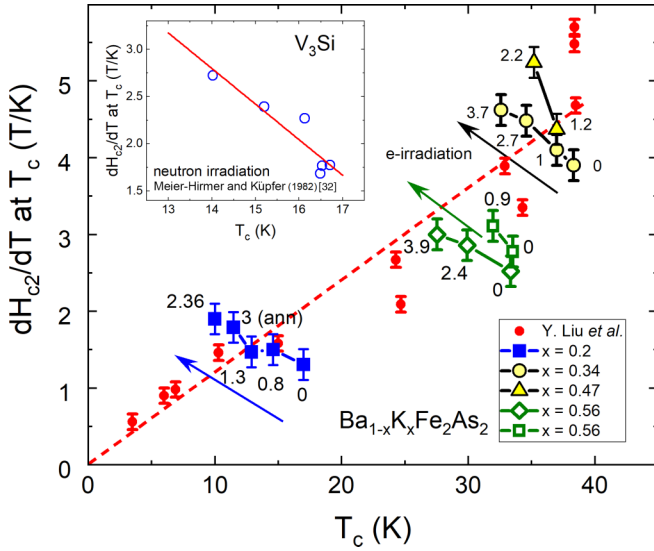


FIG. 9. The experimental slope of the upper critical field. Red symbols show many different compositions in their pristine state, from the study by Liu *et al.* [56]. As expected from the BCS theory, the slope is proportional to  $T_c$ . Blue, green, and yellow symbols show the slope change with electron irradiation (e-irradiation) for the compositions indicated in the legend. The numbers next to symbols are the doses in  $\text{C}/\text{cm}^2$ . The inset shows a similar behavior in a known two-band  $s_{++}$  superconductor  $\text{V}_3\text{Si}$  [31] irradiated by neutrons, see Ref. [32].

in transition temperature as function of irradiation dose. As expected, the dimensionless scattering rate induced by electron irradiation is linearly proportional to the dose, at least for relatively small doses, and  $T_c$  is also linearly suppressed with  $P$ . We remind the reader that here the suppression of  $T_c$  is by nonmagnetic defects and therefore only due to the anisotropy of the order parameter described by the  $\Omega$  functions of our two-band system, Eq. (8).

The lower panel of Fig. 8 shows the measured  $H_{c2}$  before and after irradiating the indicated compounds. The slope was evaluated as a derivative of each curve. A summary of the results is presented in Fig. 9. The blue, green, and yellow symbols show the slope change with electron irradiation for the compositions indicated in the legend. The numbers next to the symbols are the doses in  $\text{C}/\text{cm}^2$ . The slope  $S$  increases with decreasing transition temperature, proportional to the scattering rate  $P$ . For comparison, the inset in Fig. 9 shows similar data for the known two-band  $s_{++}$  superconductor  $\text{V}_3\text{Si}$  [31] irradiated by neutrons [32]. The slope  $S$  increases as expected from our model. This behavior is contrasted with the red symbols (main panel) showing the slope  $S$  as a function of  $T_c$  in the pristine compositions of  $\text{Ba}_{1-x}\text{K}_x\text{Fe}_2\text{As}_2$ , revealing what is expected from the BCS theory,  $S \propto T_c$  [25].

In another experiment on a single crystal of  $(\text{Ba}_{0.75}\text{K}_{0.25})\text{Fe}_2\text{As}_2$  ( $T_{c0} \approx 30.3$  K), 2.5 MeV electron irradiation was pushed to a very large dose of  $8.93 \text{ C}/\text{cm}^2 = 5.6 \times 10^{19}$  electrons/ $\text{cm}^2$ . To put this in perspective, a typical overnight irradiation run yields around  $0.8 \text{ C}/\text{cm}^2$ ; so  $8.93 \text{ C}/\text{cm}^2$  would be achieved in about 5 days of continuous irradiation, which is impossible to do in one run. It took about 2 weeks of active irradiation spread over several sessions

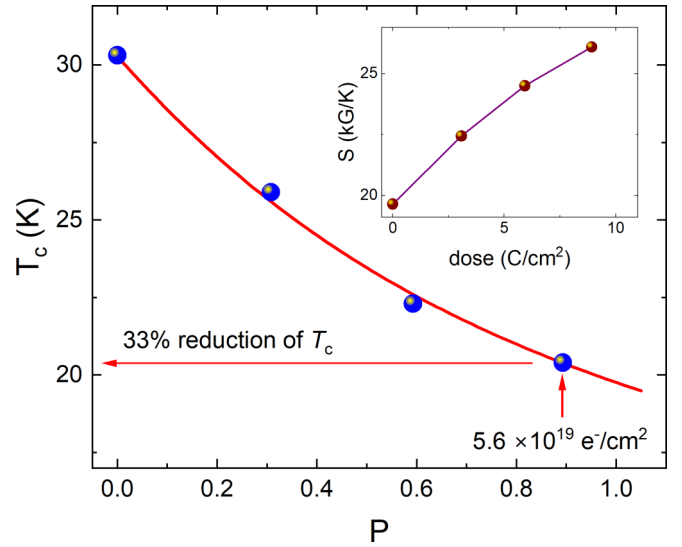


FIG. 10. Superconducting transition temperature  $T_c$  vs non-magnetic scattering rate  $P$ . Symbols are the experimental values obtained on nearly optimally doped  $\text{Ba}_{1-x}\text{K}_x\text{Fe}_2\text{As}_2$  crystal irradiated with doses of  $3.08 \text{ C}/\text{cm}^2$  ( $1.92 \times 10^{19}$  electrons/ $\text{cm}^2$ ),  $5.93 \text{ C}/\text{cm}^2$  ( $3.70 \times 10^{19}$  electrons/ $\text{cm}^2$ ), and  $8.93 \text{ C}/\text{cm}^2$  ( $5.57 \times 10^{19}$  electrons/ $\text{cm}^2$ ). The solid red curve is a fit to Eq. (1), with  $s_{++}$  pairing parameters,  $n = 0.3$ , and  $r = 2.95$  with  $v = 1$  kept constant. The inset shows the slope  $S$  as function of the irradiation dose.

that lasted a few years. As shown in Fig. 10, this level of irradiation has suppressed the transition temperature to 20.4 K – a reduction of about 33%.

In  $\text{BaFe}_2\text{As}_2$ , threshold energies of ion knock-out upon head-on collisions,  $E_d$ , were calculated using Vienna *ab initio* simulation package molecular dynamics (VASP-MD) simulations that produced  $E_d = 33$  eV (Ba), 22 eV (Fe), and 50 eV (As) [61]. With these numbers, we used the SECTE software (for details, see Ref. [61]) to calculate the total cross section of defect production upon electron irradiation,  $\sigma = 80$  b at 2.5 MeV. This gives  $5 \times 10^{-4}$  defects per atom (dpa) per  $1 \text{ C}/\text{cm}^2$ . For our highest dose of  $8.93 \text{ C}/\text{cm}^2$  we estimate  $4.5 \times 10^{-3}$  dpa or 0.045 defects per conventional unit cell ( $Z = 2$ ). This means that we produce one defect per 22.2 conventional unit cells at this dose. Therefore, with the volume of the unit cell of  $0.20457 \text{ nm}^3$ , the average distance between the defects is 1.66 nm. This should be compared with the coherence length  $\xi$  and the BCS coherence length  $\xi_0 = \hbar v_F / \pi \Delta_0$  [62].  $\text{Ba}_{1-x}\text{K}_x\text{Fe}_2\text{As}_2$  at the optimal doping,  $x = 0.4$ ,  $T_c = 38$  K, has  $H_{c2}$  with  $H \parallel c$  axis of about 150 T, while our somewhat underdoped sample has  $H_{c2} = 70$  T [56]. Therefore, while the optimal composition would have  $\xi = \sqrt{\phi_0 / 2\pi H_{c2}} \approx 1.5$  nm, our underdoped sample gives  $\xi = 2.2$  nm, both comparable to the estimated interdefect distance. Away from optimal doping, the upper critical field and transition temperature  $T_c$  decrease substantially, which means that these compositions will be deeper in the dirty limit since the scattering rate  $P \propto \xi_0 / \ell$ , where  $\ell$  is the mean free path,  $\ell \propto \text{dpa}$ . With  $\hbar v_F \sim 0.7 \text{ eV} \text{ \AA}$ , the BCS coherence length,  $\xi_0 \approx 209.88 \hbar v_F (\text{eV} \text{ \AA}) / T_c (\text{K})$ , is about 4 nm at optimal doping and approximately 5 nm for our  $x = 0.25$ . Therefore, in this paper, we expect  $P \lesssim 1$  for all

irradiation doses, which is precisely what we obtain in Fig. 10, which shows the experimental transition temperature  $T_c$  as a function of the scattering rate  $P$  (symbols) and the fit to Eq. (1) with  $\Omega$  described by  $s_{++}$  parameters,  $n = 0.3$ , and  $r = +2.95$  with  $v = 1$  (kept constant). Due to the high irradiation dose,  $T_c$  decreased substantially, by 33% at the highest dose of  $8.93 \text{ C/cm}^2$  ( $5.57 \times 10^{19}$  electrons/cm $^2$ ). The intermediate doses were  $3.08 \text{ C/cm}^2$  ( $1.92 \times 10^{19}$  electrons/cm $^2$ ) and  $5.93 \text{ C/cm}^2$  ( $3.70 \times 10^{19}$  electrons/cm $^2$ ). The inset in Fig. 10 shows that the slope  $S$  increases with the scattering rate  $P$ , as expected for an  $s_{++}$  pairing from the above theory.

## VI. DISCUSSION

Thus far, we can state that unless an  $s_{\pm}$  superconductor has very imbalanced partial densities of states of the order of 10% or less, it will show a reduction of the slope of  $H_{c2}$  at  $T_c$  with transport (nonmagnetic) disorder. An increasing slope, including an anisotropic multiband case, is predicted for any  $s_{++}$  state. Note, however, that the initial change in  $dS/dP$  becomes negative for a large difference between the gap amplitudes and small  $n$ ; see the upper left corner of Fig. 3(b).

Our data for  $\text{Ba}_{1-x}\text{K}_x\text{Fe}_2\text{As}_2$  show that the slope  $S$  increases with  $P$  across the  $T_c(x)$  dome of superconductivity for underdoped, optimally doped, and overdoped compositions. This is a strong argument in favor of multiband  $s_{++}$  superconductivity with a significant difference between different gaps. The literature review of the past two decades shows no experimental reports, at least for  $\text{Ba}_{1-x}\text{K}_x\text{Fe}_2\text{As}_2$ , that could not be explained from the anisotropic  $s_{++}$  point of view. This includes suppression of  $T_c$ , nonexponential London penetration depth, specific heat, thermal conductivity, and other transport and thermodynamic quantities. Angle-resolved photoemission is not sensitive to the sign of the order parameter but produced important information regarding the gaps' anisotropy on separate sheets of the Fermi surface [8–11]. Importantly, most works find

a fully gapped robust superconductivity in  $\text{BaK122}$  except for the end-member,  $\text{KFe}_2\text{As}_2$ , which is nodal [63,64] and lies behind the Lifshitz transition. The only phase-sensitive experiment that directly confirmed  $s_{\pm}$  superconductivity, an experiment involving quasiparticle interference, was only successfully performed on chalcogenides [65,66], distant cousins of the pnictides.

Of course, the question of the pairing type is complicated and requires considering various independent experiments and theories. For example, tunneling spectroscopy and neutron resonance studies [67] provide important information directly related to the nature of the interactions in the system. Although our approach is based on a general Ginzburg-Landau treatment of the upper critical field at  $T_c$ , our two-band model is simple. Perhaps a more elaborate microscopic theory would improve our conclusions, but we expect similar qualitative results. It is the experiment that showed the opposite trend to what is predicted for an  $s_{\pm}$  superconductor. Do we have a smoking gun that proves without a doubt the  $s_{++}$  pairing in  $\text{Ba}_{1-x}\text{K}_x\text{Fe}_2\text{As}_2$ ? No, we do not, but what seems commonly accepted is now reopened for a more in-depth discussion.

## ACKNOWLEDGMENTS

We thank P. Hirschfeld, A. Chubukov, and T. Hanaguri for useful discussions. We thank Y. Liu and T. Lograsso for providing high-quality single crystals of  $\text{Ba}_{1-x}\text{K}_x\text{Fe}_2\text{As}_2$ . This work was supported by the U.S. Department of Energy (DOE), Office of Science, Basic Energy Sciences, Materials Science and Engineering Division. Ames National Laboratory is operated for the U.S. DOE by Iowa State University under Contract No. DE-AC02-07CH11358. We thank the SIRIUS team, O. Cavani, B. Boizot, V. Metayer, and J. Losco, for running the electron irradiation experiments at École Polytechnique, Palaiseau, France. The irradiation was supported by the EMIR&A network, under User Proposal No. 11-11-0121.

- 
- [1] R. T. Gordon, H. Kim, M. A. Tanatar, R. Prozorov, and V. G. Kogan, *Phys. Rev. B* **81**, 180501(R) (2010).
- [2] V. G. Kogan, C. Martin, and R. Prozorov, *Phys. Rev. B* **80**, 014507 (2009).
- [3] W. R. Meier, T. Kong, U. S. Kaluarachchi, V. Taufour, N. H. Jo, G. Drachuck, A. E. Böhmer, S. M. Saunders, A. Sapkota, A. Kreyssig, M. A. Tanatar, R. Prozorov, A. I. Goldman, F. F. Balakirev, A. Gurevich, S. L. Bud'ko, and P. C. Canfield, *Phys. Rev. B* **94**, 064501 (2016).
- [4] P. W. Anderson, *J. Phys. Chem. Solids* **11**, 26 (1959).
- [5] A. Golubov and I. Mazin, *Physica C* **243**, 153 (1995).
- [6] I. I. Mazin, D. J. Singh, M. D. Johannes, and M. H. Du, *Phys. Rev. Lett.* **101**, 057003 (2008).
- [7] K. Kuroki, S. Onari, R. Arita, H. Usui, Y. Tanaka, H. Kontani, and H. Aoki, *Phys. Rev. Lett.* **101**, 087004 (2008).
- [8] H. Ding, P. Richard, K. Nakayama, K. Sugawara, T. Arakane, Y. Sekiba, A. Takayama, S. Souma, T. Sato, T. Takahashi, Z. Wang, X. Dai, Z. Fang, G. F. Chen, J. L. Luo, and N. L. Wang, *Europhys. Lett.* **83**, 47001 (2008).
- [9] S. V. Borisenko, V. B. Zabolotnyy, D. V. Evtushinsky, T. K. Kim, I. V. Morozov, A. N. Yaresko, A. A. Kordyuk, G. Behr, A. Vasiliev, R. Follath, and B. Büchner, *Phys. Rev. Lett.* **105**, 067002 (2010).
- [10] K. Okazaki, Y. Ota, Y. Kotani, W. Malaeb, Y. Ishida, T. Shimojima, T. Kiss, S. Watanabe, C.-T. Chen, K. Kihou, C. H. Lee, A. Iyo, H. Eisaki, T. Saito, H. Fukazawa, Y. Kohori, K. Hashimoto, T. Shibauchi, Y. Matsuda, H. Ikeda *et al.*, *Science* **337**, 1314 (2012).
- [11] K. Umezawa, Y. Li, H. Miao, K. Nakayama, Z.-H. Liu, P. Richard, T. Sato, J. B. He, D.-M. Wang, G. F. Chen, H. Ding, T. Takahashi, and S.-C. Wang, *Phys. Rev. Lett.* **108**, 037002 (2012).
- [12] D. Mou, T. Kong, W. R. Meier, F. Lochner, L.-L. Wang, Q. Lin, Y. Wu, S. L. Bud'ko, I. Eremin, D. D. Johnson, P. C. Canfield, and A. Kaminski, *Phys. Rev. Lett.* **117**, 277001 (2016).

- [13] T. Shimojima, W. Malaeb, A. Nakamura, T. Kondo, K. Kihou, C.-H. Lee, A. Iyo, H. Eisaki, S. Ishida, M. Nakajima, S. Uchida, K. Ohgushi, K. Ishizaka, and S. Shin, *Sci. Adv.* **3**, e1700466 (2017).
- [14] I. I. Mazin and J. Schmalian, *Physica C* **469**, 614 (2009).
- [15] D. C. Johnston, *Adv. Phys.* **59**, 803 (2010).
- [16] J. Paglione and R. L. Greene, *Nat. Phys.* **6**, 645 (2010).
- [17] P. J. Hirschfeld, M. M. Korshunov, and I. I. Mazin, *Rep. Prog. Phys.* **74**, 124508 (2011).
- [18] A. Chubukov, *Annu. Rev. Condens. Matter Phys.* **3**, 57 (2012).
- [19] A. Chubukov and P. J. Hirschfeld, *Phys. Today* **68**(6), 46 (2015).
- [20] H. Kontani, Y. Inoue, T. Saito, Y. Yamakawa, and S. Onari, *Solid State Commun.* **152**, 718 (2012).
- [21] V. Shestakov, M. Korshunov, and O. Dolgov, *Symmetry* **10**, 323 (2018).
- [22] D. V. Efremov, M. M. Korshunov, O. V. Dolgov, A. A. Golubov, and P. J. Hirschfeld, *Phys. Rev. B* **84**, 180512(R) (2011).
- [23] G. Ghigo, D. Torsello, G. A. Ummarino, L. Gozzelino, M. A. Tanatar, R. Prozorov, and P. C. Canfield, *Phys. Rev. Lett.* **121**, 107001 (2018).
- [24] S. Onari and H. Kontani, *Physica C* **470**, 1007 (2010).
- [25] V. G. Kogan and R. Prozorov, *Phys. Rev. B* **108**, 064502 (2023).
- [26] E. Helfand and N. R. Werthamer, *Phys. Rev.* **147**, 288 (1966).
- [27] E. Helfand and N. R. Werthamer, *Phys. Rev. Lett.* **13**, 686 (1964).
- [28] N. R. Werthamer, E. Helfand, and P. C. Hohenberg, *Phys. Rev.* **147**, 295 (1966).
- [29] S. V. Pokrovsky and V. L. Pokrovsky, *Phys. Rev. B* **54**, 13275 (1996).
- [30] N. P. Shabanova, S. I. Krasnosvobodtsev, A. V. Varlashkin, V. S. Nozdrin, and A. I. Golovashkin, *Phys. Solid State* **50**, 1397 (2008).
- [31] K. Cho, M. Kończykowski, S. Ghimire, M. A. Tanatar, L.-L. Wang, V. G. Kogan, and R. Prozorov, *Phys. Rev. B* **105**, 024506 (2022).
- [32] R. Meier-Hirmer and H. K pfer, *J. Nucl. Mater.* **108-109**, 593 (1982).
- [33] A. V. Antonov, A. V. Ikonnikov, D. V. Masterov, A. N. Mikhaylov, S. V. Morozov, Y. N. Nozdrin, S. A. Pavlov, A. E. Parafin, D. I. Tetel'baum, S. S. Ustavshchikov, V. K. Vasiliev, P. A. Yunin, and D. A. Savinov, *Physica C* **568**, 1353581 (2020).
- [34] T. B. Charikova, N. G. Shelushinina, G. I. Kharus, O. E. Sochinskaya, and A. A. Ivanov, *Phys. Solid State* **51**, 2229 (2009).
- [35] W. N. Hardy, D. A. Bonn, D. C. Morgan, R. Liang, and K. Zhang, *Phys. Rev. Lett.* **70**, 3999 (1993).
- [36] R. Prozorov, R. W. Giannetta, P. Fournier, and R. L. Greene, *Physica C* **341-348**, 1703 (2000).
- [37] S. Tokuta and A. Yamamoto, *APL Mater.* **7**, 111107 (2019).
- [38] A. E. Karkin, T. Wolf, and B. N. Goshchitskii, *J. Phys.: Condens. Matter* **26**, 275702 (2014).
- [39] K. Cho, M. Kończykowski, S. Teknowijoyo, M. A. Tanatar, and R. Prozorov, *Supercond. Sci. Technol.* **31**, 064002 (2018).
- [40] A. A. Abrikosov and L. P. Gor'kov, *Zh. Eksp. Teor. Fiz.* **39**, 1781 (1960) [*Sov. Phys. JETP* **12**, 1243 (1961)].
- [41] L. A. Openov, *Phys. Rev. B* **58**, 9468 (1998).
- [42] V. G. Kogan, *Phys. Rev. B* **80**, 214532 (2009).
- [43] E. I. Timmons, S. Teknowijoyo, M. Kończykowski, O. Cavani, M. A. Tanatar, S. Ghimire, K. Cho, Y. Lee, L. Ke, N. H. Jo, S. L. Bud'ko, P. C. Canfield, P. P. Orth, M. S. Scheurer, and R. Prozorov, *Phys. Rev. Res.* **2**, 023140 (2020).
- [44] M. Kończykowski (private communication).
- [45] K. Hashimoto, K. Cho, T. Shibauchi, S. Kasahara, Y. Mizukami, R. Katsumata, Y. Tsuruhara, T. Terashima, H. Ikeda, M. A. Tanatar, H. Kitano, N. Salovich, R. W. Giannetta, P. Walmsley, A. Carrington, R. Prozorov, and Y. Matsuda, *Science* **336**, 1554 (2012).
- [46] C. Tarantini, K. Iida, N. Sumiya, M. Chihara, T. Hatano, H. Ikuta, R. K. Singh, N. Newman, and D. C. Larbalestier, *Supercond. Sci. Technol.* **31**, 034002 (2018).
- [47] C. Tarantini, A. Gurevich, J. Jaroszynski, F. Balakirev, E. Bellingeri, I. Pallecchi, C. Ferdeghini, B. Shen, H. H. Wen, and D. C. Larbalestier, *Phys. Rev. B* **84**, 184522 (2011).
- [48] D. Markowitz and L. P. Kadanoff, *Phys. Rev.* **131**, 563 (1963).
- [49] V. L. Pokrovskii, *Zh. Eksp. Teor. Fiz.* **40**, 641 (1961) [*Sov. Phys. JETP* **13**, 447 (1961)].
- [50] V. G. Kogan, *Phys. Rev. B* **66**, 020509(R) (2002).
- [51] V. G. Kogan and R. Prozorov, *Phys. Rev. B* **103**, 054502 (2021).
- [52] R. Prozorov and V. G. Kogan, *Rep. Prog. Phys.* **74**, 124505 (2011).
- [53] I. I. Mazin, *Nature (London)* **464**, 183 (2010).
- [54] Z. P. Yin, K. Haule, and G. Kotliar, *Nat. Mater.* **10**, 932 (2011).
- [55] Y. Liu, M. A. Tanatar, V. G. Kogan, H. Kim, T. A. Lograsso, and R. Prozorov, *Phys. Rev. B* **87**, 134513 (2013).
- [56] Y. Liu, M. A. Tanatar, W. E. Straszheim, B. Jensen, K. W. Dennis, R. W. McCallum, V. G. Kogan, R. Prozorov, and T. A. Lograsso, *Phys. Rev. B* **89**, 134504 (2014).
- [57] K. Cho, M. Kończykowski, S. Teknowijoyo, M. A. Tanatar, Y. Liu, T. A. Lograsso, W. E. Straszheim, V. Mishra, S. Maiti, P. J. Hirschfeld, and R. Prozorov, *Sci. Adv.* **2**, e1600807 (2016).
- [58] M. A. Tanatar, N. Ni, S. L. Bud'ko, P. C. Canfield, and R. Prozorov, *Supercond. Sci. Technol.* **23**, 054002 (2010).
- [59] A. C. Damask and G. J. Dienes, *Point Defects in Metals* (Gordon and Breach, New York, 1963).
- [60] M. W. Thompson, *Defects and Radiation Damage in Metals*, Cambridge Monographs on Physics (Cambridge University Press, Cambridge, 1974).
- [61] K. Cho, M. Kończykowski, M. A. Tanatar, I. I. Mazin, Y. Liu, T. A. Lograsso, and R. Prozorov, *Materials* **16**, 4520 (2023).
- [62] M. Tinkham, *Introduction to Superconductivity*, 2nd ed., Dover Books on Physics (Dover, New York, 2004).
- [63] H. Fukazawa, Y. Yamada, K. Kondo, T. Saito, Y. Kohori, K. Kuga, Y. Matsumoto, S. Nakatsuji, H. Kito, P. M. Shirage, K. Kihou, N. Takeshita, C.-H. Lee, A. Iyo, and H. Eisaki, *J. Phys. Soc. Jpn.* **78**, 083712 (2009).
- [64] J.-P. Reid, M. A. Tanatar, A. Juneau-Fecteau, R. T. Gordon, S. R. de Cotret, N. Doiron-Leyraud, T. Saito, H. Fukazawa, Y. Kohori, K. Kihou, C. H. Lee, A. Iyo, H. Eisaki, R. Prozorov, and L. Taillefer, *Phys. Rev. Lett.* **109**, 087001 (2012).
- [65] T. Hanaguri, S. Niitaka, K. Kuroki, and H. Takagi, *Science* **328**, 474 (2010).
- [66] P. O. Sprau, A. Kostin, A. Kreisel, A. E. B hmer, V. Taufour, P. C. Canfield, S. Mukherjee, P. J. Hirschfeld, B. M. Andersen, and J. C. S. Davis, *Science* **357**, 75 (2017).
- [67] D. J. Scalapino, *Rev. Mod. Phys.* **84**, 1383 (2012).